NANO LETTERS

pubs.acs.org/NanoLett Letter

Plasmonic Response of Complex Nanoparticle Assemblies

Zachary M. Sherman, Kihoon Kim,[§] Jiho Kang,[§] Benjamin J. Roman, Hannah S. N. Crory, Diana L. Conrad, Stephanie A. Valenzuela, Emily Lin, Manuel N. Dominguez, Stephen L. Gibbs, Eric V. Anslyn,* Delia J. Milliron,* and Thomas M. Truskett*

Cite This: *Nano Lett.* 2023, 23, 3030−3037 Read Online

ACCESS | Metrics & More | Article Recommendations | Supporting Information

ABSTRACT: Optical properties of nanoparticle assemblies reflect distinctive characteristics of their building blocks and spatial organization, giving rise to emergent phenomena. Integrated experimental and computational studies have established design principles connecting the structure to properties for assembled clusters and superlattices. However, conventional electromagnetic simulations are too computationally expensive to treat more complex assemblies. Here we establish a fast, materials agnostic method to simulate the optical response of large nanoparticle assemblies incorporating both structural and compositional complexity. This many-bodied, mutual polarization method resolves limitations of established approaches, achieving rapid, accurate convergence for configurations including thousands of nanoparticles, with some overlapping. We demonstrate these capabilities by reproducing experimental trends and uncovering far- and near-field mechanisms governing the optical response of plasmonic semiconductor nanocrystal assemblies including structurally complex gel networks and compositionally complex mixed binary superlattices. This broadly applicable framework will facilitate the design of complex, hierarchically structured, and dynamic assemblies for desired optical characteristics.

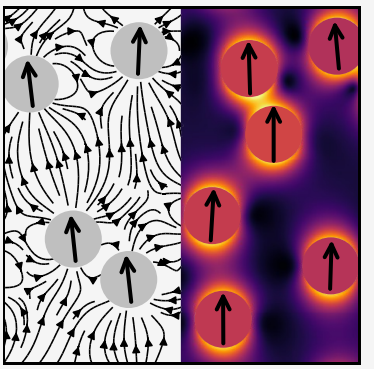

KEYWORDS: *plasmonic nanoparticles, electromagnetic simulation, mutual polarization, self-assembly, superlattice, colloidal gel*

The tunable optical response of plasmonic nanoparticle assemblies makes them attractive for applications, including sensing,[1,2] energy conversion,[3−5] and theranostics.[6,7] Developing and employing methods for electrodynamics simulation of metallic nanoparticle assemblies are essential for advancing conceptual understanding and design. The resonant interaction of free charge carriers in nanoparticles with light (localized surface plasmon resonance, LSPR) results in strong electromagnetic near-fields and enhanced absorption and scattering.[8,9] Due to LSPR coupling, the spectral response of plasmonic assemblies is sensitive to the nanoparticle spatial arrangement, i.e., structure, with amplified electromagnetic fields or hot spots in the gaps between closely spaced nanoparticles.[10−13] Analytical approaches such as Mie theories[14] or plasmon hybridization theory[11,15] and numerical solutions of classical electromagnetic scattering equations[10−12,16−22] have clarified the influence of nanoparticle morphology and coupling in small plasmonic clusters and periodic arrays. However, an open question is how to compute the optical response of significantly more complex assemblies with characteristic structural features involving large numbers of nanoparticles such as compositionally disordered superlattices[23−25] or gel networks.[13,26−30]

Structural complexity of extended, disordered nanoparticle assemblies poses challenges for conventional electromagnetic simulation techniques. Discretization requirements for the most flexible approaches[19,20]—discrete dipole approximation, finite difference time domain, finite element, and boundary element methods (e.g., method of moments[31])—render them too computationally demanding to simulate configurations with a large number N ($>10^3$) of nanoparticles. This shortcoming can be avoided for assemblies of spherical nanoparticles using the multisphere T-matrix method[32−36] and coupled dipole method,[37−39] both based on generalized Mie theory,[14] which do not require spatiotemporal discretization. However, even these approaches become slow to converge or fail altogether when nanoparticles touch or overlap, which inevitably occurs in large configurations generated from assembly simulations using coarse-grained models. The ability to predict the optical response of complex assemblies, including those from simulated nanoparticle configurations, is needed to match the complexity of emerging experimental systems[23−25,27,28,40] and accelerate their development.

Building on a framework from electrostatics, here we establish a mutual polarization method (MPM) capable of rapidly simulating the frequency-dependent optical response of large, complex assemblies of spherical nanoparticles with

Received: February 2, 2023
Revised: March 17, 2023
Published: March 29, 2023

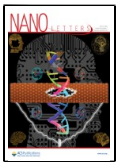

https://doi.org/10.1021/acs.nanolett.3c00429
Nano Lett. 2023, 23, 3030−3037

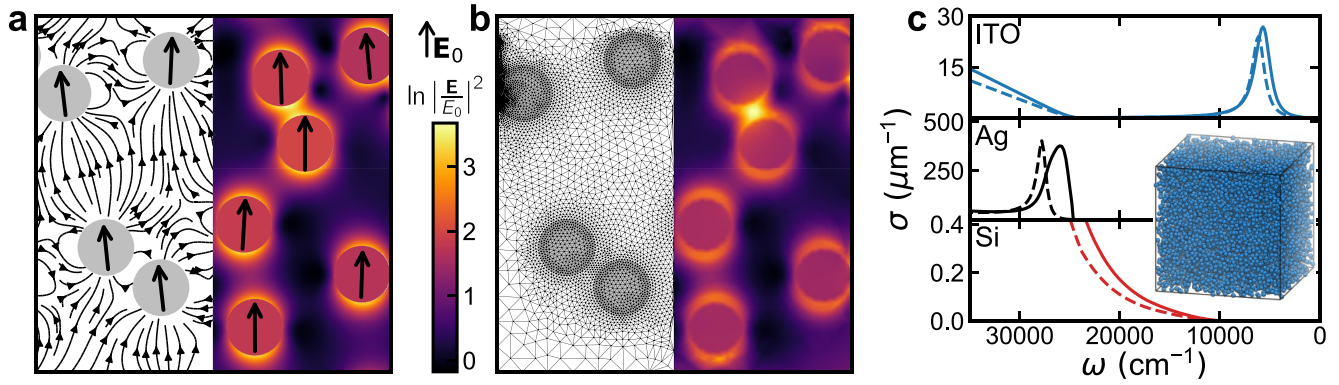

Figure 1. Broad applicability of MPM. Schematic illustrations and resultant electric field maps generated using (a) MPM and (b) finite element methods for ITO nanocrystals at an area fraction of 0.20. (c) Calculated extinction coefficients for dilute (dashed lines) and concentrated (volume fraction 0.20, solid) dispersions of ITO, silver, and silicon nanoparticles using MPM with the dielectric functions shown in Table S3. Coupling redshifts and broadens the LSPR peaks for silver and ITO at high concentration (configuration shown in inset).

arbitrary dielectric functions (Figure 1), accommodating configurations with particle overlaps and triply periodic boundary conditions. We use this approach to predict and interpret experimental spectra for disordered systems with characteristic features that comprise more nanoparticles than would be practical to analyze by conventional electromagnetic simulations: (1) two-dimensional randomly mixed binary superlattices and (2) three-dimensional nanoparticle gel networks. Our analysis shows how far-field spectral features emerge from heterogeneous, structure-dependent near-field coupling and illustrates how MPM integrates data from structural and optical measurements to provide insights into ordering across length scales in complex assemblies.

Mutual Polarization Method. MPM computes the optical response on the basis of the polarization of each particle by the incident field $\mathbf{E}_0$ and by the electric dipoles of the other $N - 1$ particles in the system. The polarization depends on the particle's composition through its dielectric function, $\varepsilon_i(\omega)$, where ω is the frequency of light. Spherical particles of any dielectric function can be treated (Figure 1c); however, here we only consider particles in the quasistatic limit, where their radius a is small compared to the wavelength of light. This simplification is broadly applicable for LSPR coupling in nanoparticle assemblies, and it allows the N particle dipole moments $\mathbf{p}_1$, ..., $\mathbf{p}_N$ to be determined by solving the electrostatics limit of Maxwell's equations, i.e., the Poisson and Laplace equations.

Like other approaches based on generalized Mie theory,[14] MPM does not require fine spatial discretization to solve the electromagnetic scattering problem, though its predictions compare favorably with those from finite element solutions (Figures 1b and S1–S3). MPM neglects multipole moments induced by local field gradients, yet it captures all significant structure-dependent trends in the far- and near-field optical response. In many cases, higher-order moments naturally captured in finite element (and comparable) methods only contribute small quantitative changes to the dipolar response (Figures S1–S3) at large additional computational expense (Figure S4). Therefore, MPM can compute the optical response of assemblies with more complex structures involving larger particle numbers than other approaches in orders of magnitude less computation time (Figure S4).

In MPM, the electric dipole of each particle i, $\mathbf{p}_i = \varepsilon_m\alpha_i(\omega)\mathbf{E}(\mathbf{x}_i)$, is expressed in terms of its dipolar polarizability, $\alpha_i(\omega) = 4\pi a^3[\varepsilon_i(\omega) - \varepsilon_m]/[\varepsilon_i(\omega) + 2\varepsilon_m]$, and the local electric field, $\mathbf{E}(\mathbf{x}) = \mathbf{E}_0 + \sum_j^N (4\pi\varepsilon_m r^3)^{-1}(3\hat{\mathbf{r}}\hat{\mathbf{r}} - \mathbf{I})\cdot\mathbf{p}_j$, which is a sum of the incident field and the fields of scattered waves and expressed to lowest order in ω. Here, ε_m is the (real and frequency-independent) permittivity of the background medium, $\mathbf{r} = \mathbf{x} - \mathbf{x}_i$, $\mathbf{x}_i$ is particle i's position, $r = |\mathbf{r}|$, $\hat{\mathbf{r}} = \mathbf{r}/r$, and $\mathbf{I}$ is the identity tensor. Other observables related to the optical response, such as frequency-dependent extinction coefficient $\sigma(\omega)$ or transmittance through a nanoparticle film, can be readily computed from these quantities (Supporting Information Sections 1.2 and 4.2).

The heart of MPM is an efficient solution of the resulting many-bodied linear system of equations for the N particle dipoles:

$$\mathbf{E}_0 = \sum_j^N \mathbf{M}_{ij}\cdot\mathbf{p}_j \tag{1}$$

Here, we have introduced a scattering matrix with elements $\mathbf{M}_{ij}$:

$$\mathbf{M}_{ij} = \begin{cases} \frac{1}{\varepsilon_m\alpha_i}\mathbf{I} & i = j \\ \frac{1}{4\pi\varepsilon_m r_{ij}^3}(\mathbf{I} - 3\hat{\mathbf{r}}_{ij}\hat{\mathbf{r}}_{ij}) & i \neq j,\ r_{ij} \geq 2a \\ \frac{1}{4\pi a^3\varepsilon_m}\left[\left(1 - \frac{9r_{ij}}{16a} + \frac{r_{ij}^3}{32a^3}\right)\mathbf{I}\right. & \\ \left. + \left(\frac{3r_{ij}^3}{32a^3} - \frac{9r_{ij}}{16a}\right)\hat{\mathbf{r}}_{ij}\hat{\mathbf{r}}_{ij}\right] & i \neq j,\ r_{ij} < 2a \end{cases} \tag{2}$$

constructed to avoid singularities, unphysical property predictions, and convergence problems when solving for dipoles of particles with overlapping optical cores, $r_{ij} < 2a$ (Figures S5 and S6). Overlaps naturally occur in simulated assemblies due to coarse-grained model nanoparticle interactions, but this scattering matrix is readily inverted to obtain well-behaved solutions of eq 1 for any spatial arrangement of particles. Similar regularization strategies have been applied to treat overlaps while simulating many-bodied hydrodynamic[41,42] and magnetic[43,44] forces in colloidal suspensions, which also require assigning sharp particle interfaces (for continuum properties) together with soft-particle interactions (for

https://doi.org/10.1021/acs.nanolett.3c00429
Nano Lett. 2023, 23, 3030−3037

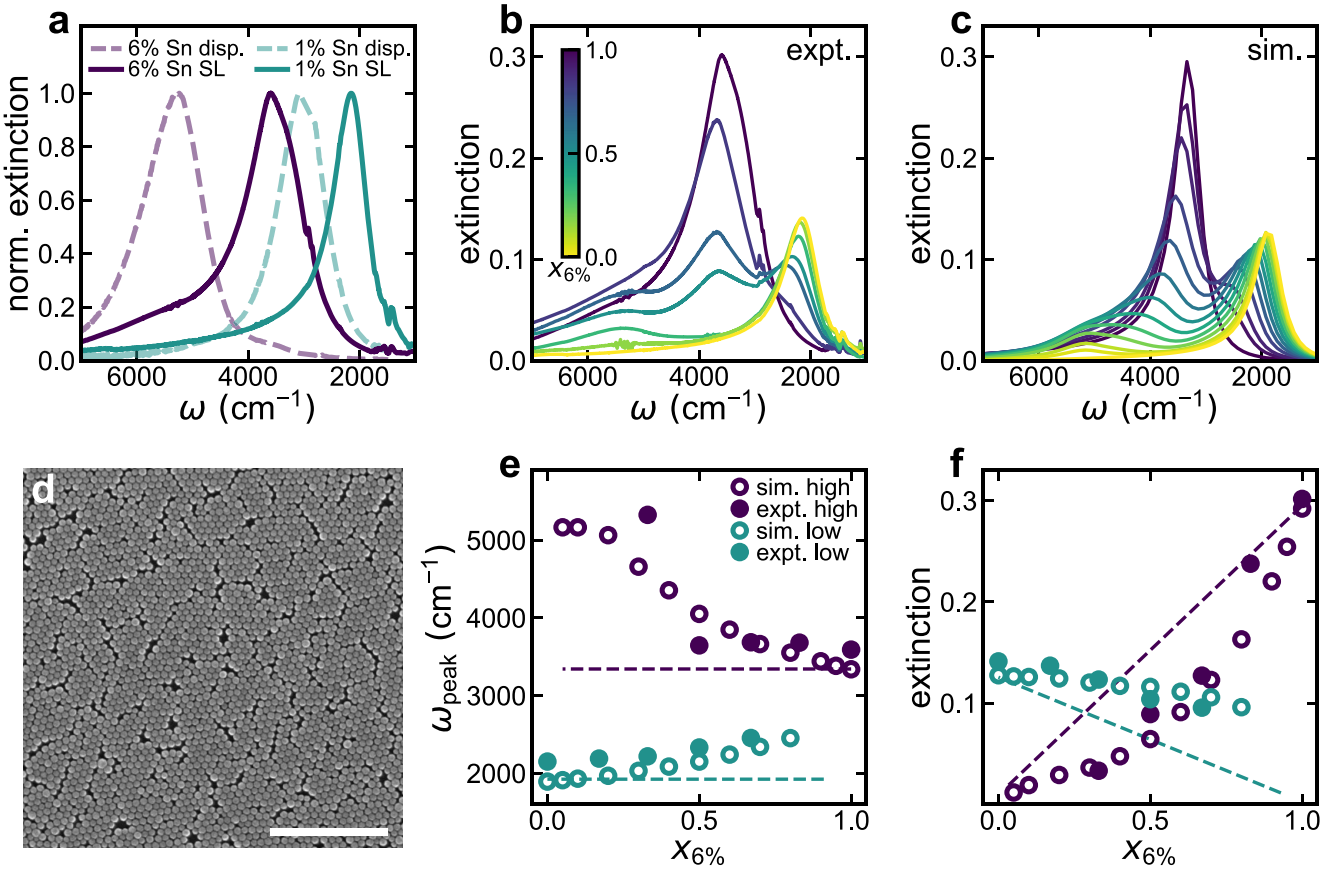

Figure 2. Spectral response of mixed ITO nanocrystal superlattices. (a) Experimental extinction spectra for nanocrystal dispersions (dashed) and single-component superlattices (solid). (b) Experimental and (c) simulated extinction spectra for various compositions $x_{6\%}$ of mixed superlattices. (d) Scanning electron micrograph of a mixed superlattice comprising 1% Sn and 6% Sn ITO nanocrystals (scale bar 500 nm). (e) Extinction peak locations ω_{peak} and (f) heights of the high-frequency (high) and low-frequency (low) peaks in (b) and (c) as a function of $x_{6\%}$. The dashed lines indicate the values that would result from simple linear mixing of the pure 6% and pure 1% superlattice spectra.

dynamics). For triply periodic geometries, $\mathbf{M}_{ij}$ can be expressed in a compact form (Figure S3) amenable to a highly efficient, matrix-free, and spectrally accurate Ewald summation method[45] that allows the linear system for dipoles to be solved rapidly using iterative schemes (Figure S4). The system of eqs 1 and 2 is similar to that in coupled dipole methods, but our approach differs by regularizing dipoles as particles overlap and in our matrix-free spectral Ewald summation method for evaluating the right-hand side of eq 1. Therefore, MPM avoids the convergence and ill-conditioning issues that plague traditional coupled dipole methods[37−39] when dipoles are close to one another (Figures S5 and S6), allowing for rapid calculations on arbitrary particle configurations that can be obtained from molecular simulation, including those for which coupled dipole methods fail or are too slow. Our spectral Ewald summation is a comparable alternative to fast multipole methods, which also rapidly solve equations similar to eqs 1−2.[31,46,47] MPM code is available at github.com/zeesherman/mutual-polarization.

Mixed Nanocrystal Superlattices. To demonstrate the utility of MPM for design of compositionally complex nanoparticle assemblies, we analyze the collective optical response of mixed nanocrystal superlattices, where the mixing ratio allows continuous tuning of effective properties. Tin-doped indium oxide (ITO) nanocrystals have a near-ideal metallic dielectric function with a tunable LSPR depending on the chosen dopant concentration (% Sn). Consistent with previous reports of other nanocrystal compositions,[23−25] we found that ITO nanocrystals with different % Sn readily form intermixed two-dimensional hexagonal superlattices, as long as their sizes are closely matched (here, $a \approx 15$ nm, Figures 2d, S7, and S8).

At infrared wavelengths, the ITO permittivity is well-described by a simple Drude dielectric function:

$$\varepsilon_p(\omega) = \varepsilon_\infty - \frac{\varepsilon_0 \omega_p^2}{\omega^2 + i\gamma\omega} \tag{3}$$

where ε_∞ is the high-frequency permittivity, set equal to $4\varepsilon_0$, while doping changes both ω_p, which primarily controls the LSPR peak position, and γ, which determines peak width. Plasmonic coupling causes a large redshift of the extinction spectrum upon assembly into a superlattice (Figure 2a). However, when scaled by ω_p, the magnitude of this shift is independent of % Sn (Table S1). In this sense, the range of attainable optical responses is limited for single-component superlattices even when the nanocrystal building blocks themselves have continuously tunable properties.

Although binary superlattices with ordered arrangements of two components[48,49] are difficult to assemble experimentally, they are simple to study computationally, because they can be modeled using a small periodic unit cell.[24,39] Conversely,

https://doi.org/10.1021/acs.nanolett.3c00429
Nano Lett. 2023, 23, 3030−3037

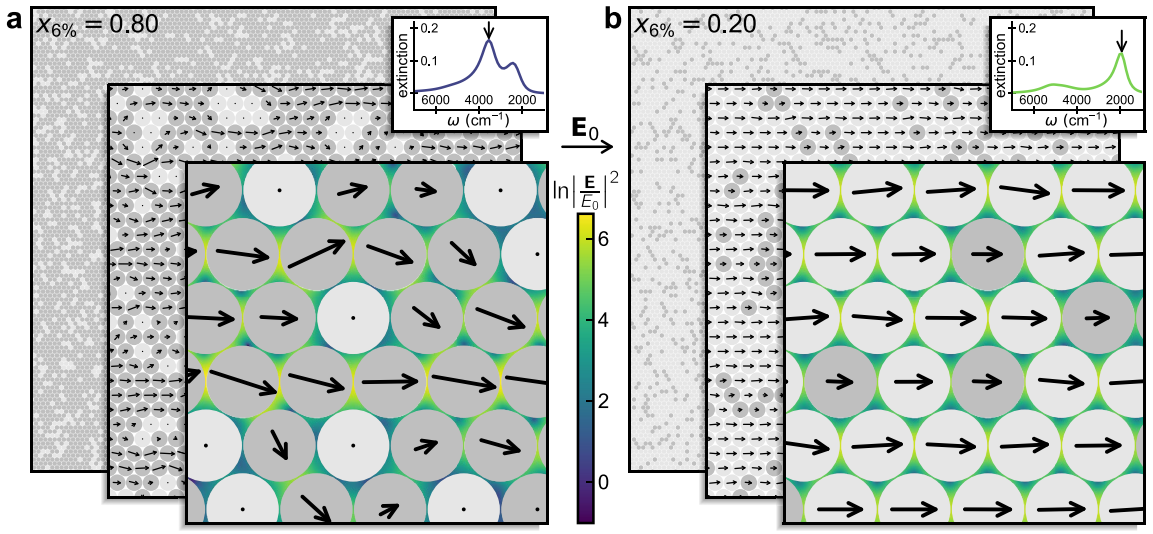

Figure 3. Electric near-field maps for mixed nanocrystal superlattices. Spatial maps of the local field intensity at (a) the high-frequency LSPR for $x_{6\%}$ = 0.80 and (b) the low-frequency LSPR for $x_{6\%}$ = 0.20. Foreground panels magnify small areas within the entire simulated configuration shown in the back panels. Dark (6% Sn) and light (1% Sn) gray indicate the nanocrystal type, and arrow lengths indicate the magnitude and direction of the imaginary part of each particle's dipole moment. Corresponding extinction spectra are inset with the excitation frequency indicated.

randomly mixed superlattices are computationally challenging; a large number of particles must be used to prevent periodic boundary conditions from imposing artificial sublattice ordering and to adequately sample the possible nanocrystal arrangements.

We vary the mixing ratio of 1% Sn and 6% Sn ITO nanocrystals in superlattices continuously, changing the fraction of 6% Sn nanocrystals, $x_{6\%}$. Qualitatively, the normal incidence extinction spectra of the mixed superlattices evolve systematically between the spectra of the two single-component assemblies, but neither the extinction spectra, the peak positions, nor the peak heights reflect simple linear mixing (Figures 2b,e,f and S9). Electron transfer is not expected to occur between nanocrystals,[50] but LSPR coupling between neighboring nanocrystals should depend on their % Sn.

These spectral trends are accurately reproduced in simulations of superlattice extinction by using MPM (Figure 2c). We model the superlattices by constructing two-dimensional hexagonal lattices containing 11600 nanocrystals, each having one of two Drude dielectric functions using parameters (ω_p and γ) determined by fitting the extinction spectra of dilute solvent dispersions of the corresponding nanocrystals (Figure S10 and Table S2).[51] Using MPM, we simulate the normal incidence extinction spectra, averaged over 2 polarizations and 20 randomly arranged superlattices. The correspondence with the experimental spectra supports our supposition that the lattices are well-mixed, with little to no phase segregation between the two types of ITO nanocrystals, an outcome that would be difficult to directly verify by electron microscopy, owing to their very similar electron densities.

As such, we interpret the shifting peak positions with composition ($x_{6\%}$) as arising from a changing average number of spectrally resonant neighboring nanocrystals (Figure 2e). For instance, compared to a pure 1% Sn superlattice ($x_{6\%}$ = 0), the lower frequency extinction peak blue-shifts with increasing $x_{6\%}$ as each 1% Sn nanocrystal has fewer 1% Sn neighbors with which to couple. The same is true of the higher frequency peak moving away from $x_{6\%}$ = 1. A third peak, around 5100 cm^{-1}, arises only for intermediate compositions, ascribed to "isolated" 6% Sn nanocrystals with relatively few 6% Sn neighbors.

Understanding the trends in peak heights (Figure 2f) requires microscopic insight made possible by visualizing the spatial variation of dipolar polarizations and local electric fields (Figure 3) and quantifying their probability distributions (Figure S11). For instance, starting from $x_{6\%}$ = 1, the intensity of the high frequency peak drops much more quickly with changing $x_{6\%}$ than would be expected from linear mixing. For a superlattice containing a fraction $x_{6\%}$ = 0.80 of 6% Sn nanocrystals, examining the dipoles induced by excitation at the peak reveals that the 1% Sn nanocrystals are effectively acting as dielectric spacers that have minimal polarization, so 6% Sn nanocrystals near 1% Sn nanocrystals have significantly reduced dipoles because they do not get a mutual polarization boost (Figure 3a). These effects weaken the overall response, reducing the extinction intensity. The field is also highly concentrated along the paths formed by 6% Sn nanocrystals, resulting in a heterogeneous distribution of field strengths and dipole orientations (Figure S11). In a superlattice with only a fraction $x_{6\%}$ = 0.20 of 6% Sn nanocrystals, conversely, the 1% Sn nanocrystals' polarization is enhanced by coupling to neighboring 1% Sn and 6% Sn nanocrystals alike, strengthening and better aligning their dipoles with the applied field (Figure 3b). As a result, the low frequency extinction peak intensity falls off more gradually than expected from linear mixing as $x_{6\%}$ increases, and the local field enhancement is more evenly distributed (Figure S11). The spectral redistribution of extinction and spatial redistribution of electric field intensity hint at a rich variety of effective metamaterial properties and near-field phenomena that could be realized in mixed nanocrystal superlattices. MPM's ability to rapidly screen a large compositional parameter space will enable the exploration of these possibilities.

Nanocrystal Gels. Nanocrystal gels have structural complexity that spans length scales, which has so far hampered the use of simulations to predict or rationalize their structure-dependent optical properties. Although plasmonic nanoparticle

https://doi.org/10.1021/acs.nanolett.3c00429
Nano Lett. 2023, 23, 3030−3037

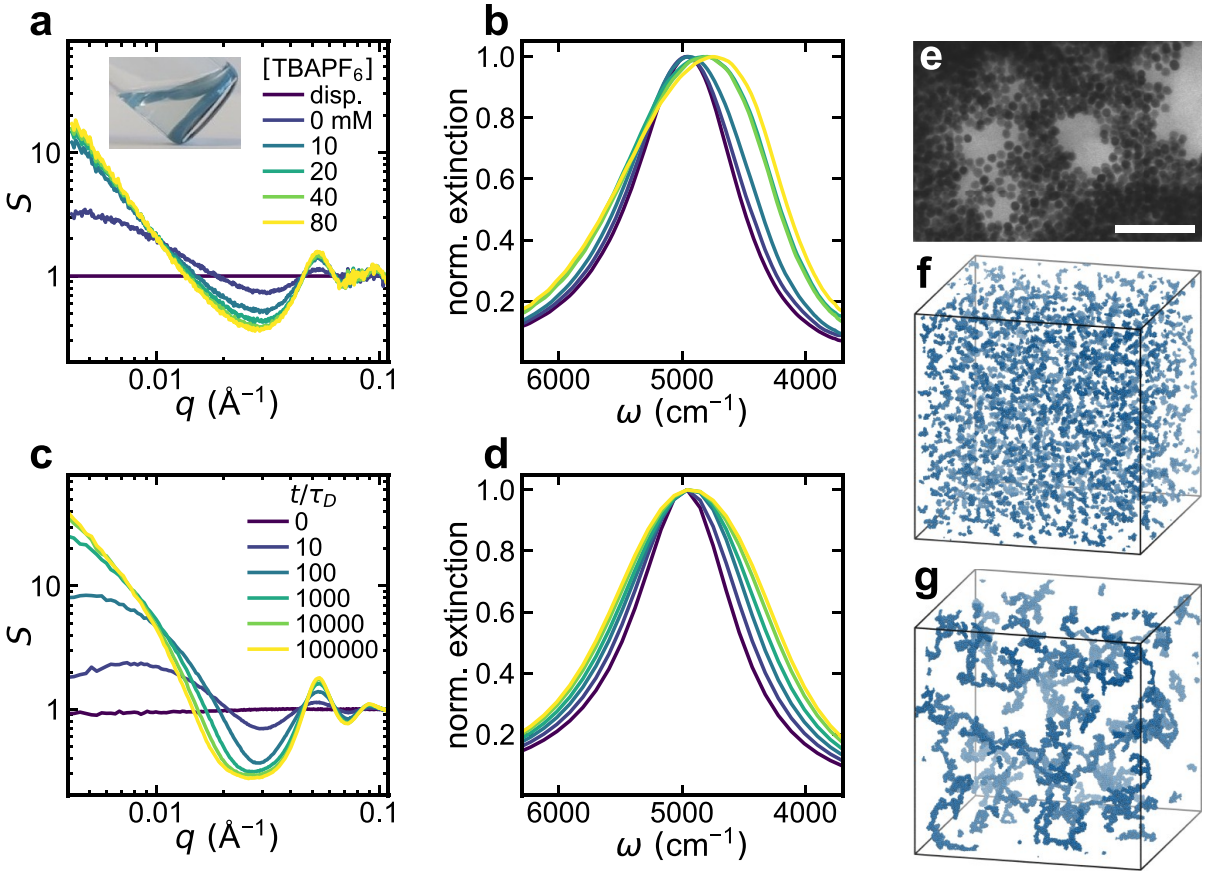

Figure 4. Structural and optical evolution of ITO nanocrystal gels. (a) Experimental SAXS stucture factors S (gel seen in blue, photo inset) and (b) extinction spectra of a dispersion and gels 11 days after preparation. Simulated (c) S and (d) extinction spectra. (e) Scanning transmission electron micrograph of a gel (scale bar, 100 nm). Simulation snapshots at coarsening times (f) $t = 1000\tau_D$ and (g) $100000\tau_D$.

gels have been reported to exhibit spectrally shifted and broadened extinction spectra compared to those of their constituent nanoparticles, these effects vary widely and unpredictably for different nanoparticle compositions and gel preparation strategies.[13,26−28] Finite element (and similar) methods are unable to capture this complexity because of the large number of nanoparticles required to represent the multiscale structure of gels.[26] We demonstrate the value of MPM for understanding gel structure and optical properties by considering networks of ITO nanocrystals ($a \approx 6$ nm, 6.0% Sn) linked by dynamic covalent bonding[27] (Figures 4, S12, and S13).

Gel structure commonly depends on sample history and preparation protocol, and we find that the structure factor S acquired by small-angle X-ray scattering (SAXS) of ITO nanocrystal gels evolves systematically with the amount of noncoordinating salt, tetrabutylammonium hexafluorophosphate ($TBAPF_6$), present during gel formation (Figures 4a and S14). The enhancement of the primary peak at wavenumber $q \sim 0.05$ Å^{-1} and progressive deepening of the minimum at lower q are reminiscent of coarsening,[52] suggesting that the salt concentration determines the extent of structural evolution approaching arrest. These features are replicated in Brownian dynamics simulations of coarsening of nanoparticles with strong, short-range attractions (Figures 4c,f,g and S15). Indeed, the S at higher [$TBAPF_6$] superposes with S for a lower [$TBAPF_6$] gel at longer aging time, supporting a correspondence between the effects of salt concentration and time (Figure S16). However, other structures, like cluster fluids of varying cluster fractal dimension, can have similar S, so S alone is not sufficient to determine the microstructural evolution (Figure S17).

The optical extinction spectra of the gels also depend on the salt concentration (Figures 4b and S18), providing complementary information to help understand their structures. At higher [$TBAPF_6$], the extinction broadens and redshifts. We used MPM to test whether coarsening can explain these changes. ITO nanocrystals in this size range are known to have a radially varying free electron concentration, so we model their dielectric function with a Drude-type plasmonic core and a dielectric shell, complexity easily incorporated into MPM. As before, the parameters describing the dielectric function are determined by fitting the LSPR spectrum of a dilute nanocrystal dispersion (Figure S10, Tables S2 and S3).[51] At various stages of coarsening from the Brownian dynamics trajectory, we use MPM to compute the polarization-averaged extinction spectrum for the 64000 nanoparticle configuration (Figure 4d). The simulations reproduce the asymmetric broadening observed experimentally, while other candidate microstructures like cluster fluids with similar trends in S show the opposite optical broadening trends (Figure S17). The local density increases by over an order of magnitude during coarsening (Figure S19), drastically changing the dipolar coupling environment and instigating the optical broadening. This example illustrates the power of MPM to combine

https://doi.org/10.1021/acs.nanolett.3c00429
Nano Lett. 2023, 23, 3030−3037

structural and optical information to provide mechanistic insights across length scales in complex assemblies.

Outlook. Building on advances presented here, MPM's computational efficiency will enable on-the-fly evaluation of optical properties in dynamic nanoparticle-based simulations, making possible the design of complex plasmonic assemblies with targeted near- or far-field responses using inverse methods.[53] Computation-guided design of disordered structures with desired optical properties is particularly compelling for soft hybrid materials (e.g., plasmonic gels)[13,26−28] that can dynamically reconfigure—modulating how they interact with light—in response to stimuli. Recently, MPM has been applied to compute the optical properties of such linked nanocrystal gel networks,[54] including under strain.[55] MPM can readily model hybrid materials comprising both dielectric (e.g., semiconductor) and metal nanoparticles or with hierarchical nanoparticle ordering, significantly expanding the design space where computation can enhance experimental discovery. An intriguing possibility is the creation of plasmonic materials with inhomogeneous electric fields in compositionally specific locations within the assembly, e.g., to enhance molecular detection sensitivity, plasmon-driven chemistry, or nonlinear optical effects.

Because MPM explicitly incorporates structure, it models optical phenomena that cannot be captured in effective medium and mean-field theories. Though the present work focuses on optical extinction and transmission, MPM can be extended to other properties of interest. One example is treating circularly polarized incident light, enabling simulation and design of plasmonic materials with chiroptical responses.[21,56] Here we established MPM at the level of quasistatic dipoles, which is sufficient to quantify the many-bodied contributions to most observations of complex assemblies. It is possible, though increasingly computationally intensive, to make MPM more quantitatively predictive by incorporating nonquasistatic dipoles with frequency-dependent scattering and incident terms in eqs 1 and 2 and by including higher-order polarization moments (quadrupoles, etc.) induced by both local and incident electric field gradients. These features are important for modeling nanoparticles that are not small compared to incident wavelengths. Finally, strategies for treating nonspherical nanoparticles have been developed as extensions to Mie theory,[14] and similar approaches may be pursued to extend MPM to handle triaxial ellipsoids or cubes.

■ ASSOCIATED CONTENT

Supporting Information

The Supporting Information is available free of charge at https://pubs.acs.org/doi/10.1021/acs.nanolett.3c00429.

Additional details of the mutual polarization method, nanocrystal synthesis and assembly, materials characterization, and other simulation aspects (PDF)

■ AUTHOR INFORMATION

Corresponding Authors

Eric V. Anslyn − *Department of Chemistry, University of Texas at Austin, Austin 78712 Texas, United States;* orcid.org/0000-0002-5137-8797; Email: anslyn@austin.utexas.edu

Delia J. Milliron − *McKetta Department of Chemical Engineering and Department of Chemistry, University of Texas at Austin, Austin 78712 Texas, United States;* orcid.org/0000-0002-8737-451X; Email: milliron@che.utexas.edu

Thomas M. Truskett − *McKetta Department of Chemical Engineering and Department of Physics, University of Texas at Austin, Austin 78712 Texas, United States;* orcid.org/0000-0002-6607-6468; Email: truskett@che.utexas.edu

Authors

Zachary M. Sherman − *McKetta Department of Chemical Engineering, University of Texas at Austin, Austin 78712 Texas, United States;* orcid.org/0000-0001-9798-287X

Kihoon Kim − *McKetta Department of Chemical Engineering, University of Texas at Austin, Austin 78712 Texas, United States;* orcid.org/0000-0003-1034-9233

Jiho Kang − *McKetta Department of Chemical Engineering, University of Texas at Austin, Austin 78712 Texas, United States*

Benjamin J. Roman − *McKetta Department of Chemical Engineering, University of Texas at Austin, Austin 78712 Texas, United States;* orcid.org/0000-0003-2213-2533

Hannah S. N. Crory − *Department of Chemistry, University of Texas at Austin, Austin 78712 Texas, United States*

Diana L. Conrad − *Department of Chemistry, University of Texas at Austin, Austin 78712 Texas, United States*

Stephanie A. Valenzuela − *Department of Chemistry, University of Texas at Austin, Austin 78712 Texas, United States*

Emily Lin − *McKetta Department of Chemical Engineering, University of Texas at Austin, Austin 78712 Texas, United States;* orcid.org/0000-0002-7189-0536

Manuel N. Dominguez − *Department of Chemistry, University of Texas at Austin, Austin 78712 Texas, United States;* orcid.org/0000-0002-9606-9234

Stephen L. Gibbs − *McKetta Department of Chemical Engineering, University of Texas at Austin, Austin 78712 Texas, United States;* orcid.org/0000-0003-2533-0957

Complete contact information is available at: https://pubs.acs.org/10.1021/acs.nanolett.3c00429

Author Contributions

[§]These authors contributed equally to this work.

Notes

The authors declare no competing financial interest.

■ ACKNOWLEDGMENTS

This research was primarily supported by the National Science Foundation through the Center for Dynamics and Control of Materials: an NSF Materials Research Science and Engineering Center (NSF MRSEC) under Cooperative Agreement DMR-1720595. E.V.A. acknowledges support from the Welch Regents Chair (F-0046). D.J.M. and T.M.T. acknowledge support from the Welch Foundation (F-1696 and F-1848) and NSF (CHE-1905263). This work was supported by an NSF Graduate Research Fellowship (DGE-1610403) to S.A.V. and Arnold O. Beckman Postdoctoral Fellowship to Z.M.S. We acknowledge the Texas Materials Institute for use of the SAXSLAB Ganesha, acquired using an NSF MRI grant CBET-1624659. We thank the Texas Advanced Computing Center (TACC) at the University of Texas at Austin for HPC resources. We thank M. Wren Berry for ICP-OES measurements and Matthew Sheldon for critical feedback on the manuscript.

REFERENCES

(1) Elghanian, R.; Storhoff, J. J.; Mucic, R. C.; Letsinger, R. L.; Mirkin, C. A. Selective colorimetric detection of polynucleotides based on the distance-dependent optical properties of gold nanoparticles. *Science* **1997**, *277*, 1078−1081.

(2) Le, F.; Brandl, D. W.; Urzhumov, Y. A.; Wang, H.; Kundu, J.; Halas, N. J.; Aizpurua, J.; Nordlander, P. Metallic nanoparticle arrays: a common substrate for both surface-enhanced Raman scattering and surface-enhanced infrared absorption. *ACS Nano* **2008**, *2*, 707−718.

(3) Atwater, H. A.; Polman, A. Plasmonics for Improved Photovoltaic Devices. *Nat. Mater.* **2010**, *9*, 205−2013.

(4) Liu, Z.; Hou, W.; Pavaskar, P.; Aykol, M.; Cronin, S. B. Plasmon resonant enhancement of photocatalytic water splitting under visible illumination. *Nano Lett.* **2011**, *11*, 1111−1116.

(5) Aslam, U.; Rao, V. G.; Chavez, S.; Linic, S. Catalytic Conversion of Solar to Chemical Energy on Plasmonic Metal Nanostructures. *Nat. Catal.* **2018**, *1*, 656−665.

(6) Lin, J.; Wang, S.; Huang, P.; Wang, Z.; Chen, S.; Niu, G.; Li, W.; He, J.; Cui, D.; Lu, G.; Chen, X.; Nie, Z. Photosensitizer-loaded gold vesicles with strong plasmonic coupling effect for imaging-guided photothermal/photodynamic therapy. *ACS Nano* **2013**, *7*, 5320−5329.

(7) Wang, S.; et al. Plasmonic Copper Sulfide Nanocrystals Exhibiting Near-Infrared Photothermal and Photodynamic Therapeutic Effects. *ACS Nano* **2015**, *9*, 1788−1800.

(8) Giannini, V.; Fernandez-Dominguez, A. I.; Heck, S. C.; Maier, S. A. Plasmonic Nanoatennas: Fundamentals and Their Use in Controlling the Radiative Properties of Nanoemitters. *Chem. Rev.* **2011**, *111*, 3888−3912.

(9) Agrawal, A.; Cho, S. H.; Zandi, O.; Ghosh, S.; Johns, R. W.; Milliron, D. J. Localized Surface Plasmon Resonance in Semiconductor Nanocrystals. *Chem. Rev.* **2018**, *118*, 3121−3207.

(10) Jain, P. K.; El-Sayed, M. A. Plasmonic coupling in noble metal nanostructures. *Chem. Phys. Lett.* **2010**, *487*, 153−164.

(11) Halas, N. J.; Lal, S.; Chang, W.-S.; Link, S.; Nordlander, P. Plasmons in strongly coupled metallic nanostructures. *Chem. Rev.* **2011**, *111*, 3913−3961.

(12) Ross, M. B.; Mirkin, C. A.; Schatz, G. C. Optical properties of one-, two-, and three-dimensional arrays of plasmonic nanostructures. *J. Phys. Chem. C* **2016**, *120*, 816−830.

(13) Pastoriza-Santos, I.; Kinnear, C.; Pérez-Juste, J.; Mulvaney, P.; Liz-Marzán, L. M. Plasmonic polymer nanocomposites. *Nat. Rev. Mater.* **2018**, *3*, 375−391.

(14) Quinten, M. *Optical properties of nanoparticle systems: Mie and beyond*, 1st ed.; Wiley-VCH: Weinheim, 2011.

(15) Prodan, E.; Radloff, C.; Halas, N. J.; Nordlander, P. A hybridization model for the plasmon response of complex nanostructures. *Science* **2003**, *302*, 419−422.

(16) Storhoff, J. J.; Lazarides, A. A.; Mucic, R. C.; Mirkin, C. A.; Letsinger, R. L.; Schatz, G. C. What controls the optical properties of DNA-linked gold nanoparticle assemblies? *J. Am. Chem. Soc.* **2000**, *122*, 4640−4650.

(17) Lazarides, A. A.; Schatz, G. C. DNA-linked metal nanosphere materials: Structural basis for the optical properties. *J. Phys. Chem. B* **2000**, *104*, 460−467.

(18) Ghosh, S. K.; Pal, T. Interparticle Coupling Effect on the Surface Plasmon Resonance of Gold Nanoparticles: From Theory to Applications. *Chem. Rev.* **2007**, *107*, 4797−4862.

(19) Myroshnychenko, V.; Rodriguez-Fernandez, J.; Pastoriza-Santos, I.; Funston, A. M.; Novo, C.; Mulvaney, P.; Liz-Marzan, L. M.; Garcia de Abajo, F. J. Modelling the optical response of gold nanoparticles. *Chem. Soc. Rev.* **2008**, *37*, 1792−1805.

(20) Wriedt, T. Light scattering theories and computer codes. *J. Quant. Spectrosc. Radiat. Transfer* **2009**, *110*, 833−843.

(21) Fan, Z.; Govorov, A. O. Plasmonic Circular Dichroism of Chiral Metal Nanoparticle Assemblies. *Nano Lett.* **2010**, *10*, 2580−2597.

(22) Hamon, C.; Novikov, S. M.; Scarabelli, L.; Solís, D. M.; Altantzis, T.; Bals, S.; Taboada, J. M.; Obelleiro, F.; Liz-Marzán, L. M. Collective Plasmonic Properties in Few-Layer Gold Nanorod Supercrystals. *ACS Photonics* **2015**, *2*, 1482−1488.

(23) Cargnello, M.; Johnston-Peck, A. C.; Diroll, B. T.; Wong, E.; Datta, B.; Damodhar, D.; Doan-Nguyen, V. V. T.; Herzing, A. A.; Kagan, C. R.; Murray, C. B. Substitutional Doping in Nanocrystal Superlattices. *Nature* **2015**, *524*, 450−453.

(24) Shi, Q.; Sikdar, D.; Fu, R.; Si, K. J.; Dong, D.; Liu, Y.; Premaratne, M.; Cheng, W. 2D Binary Plasmonic Nanoassemblies with Semiconductor n/p-Doping-Like Properties. *Adv. Mater.* **2018**, *30*, 1801118.

(25) Jishkariani, D.; Elbert, K. C.; Wu, Y.; Lee, J. D.; Hermes, M.; Wang, D.; van Blaaderen, A.; Murray, C. B. Nanocrystal Core Size and Shape Substitutional Doping and Underlying Crystalline Order in Nanocrystal Superlattices. *ACS Nano* **2019**, *13*, 5712−5719.

(26) Saez Cabezas, C. A.; Ong, G. K.; Jadrich, R. B.; Lindquist, B. A.; Agrawal, A.; Truskett, T. M.; Milliron, D. J. Gelation of Plasmonic Metal Oxide Nanocrystals by Polymer-Induced Depletion Attractions. *Proc. Natl. Acad. Sci. U.S.A.* **2018**, *115*, 8925−8930.

(27) Dominguez, M. N.; et al. Assembly of Linked Nanocrystal Colloids by Reversible Covalent Bonds. *Chem. Mater.* **2020**, *32*, 10234−10245.

(28) Kang, J.; Valenzuela, S. A.; Lin, E. Y.; Dominguez, M. N.; Sherman, Z. M.; Truskett, T. M.; Anslyn, E. V.; Milliron, D. J. Colorimetric Quantification of Linking in Thermoreversible Nanocrystal Gel Assemblies. *Sci. Adv.* **2022**, *8*, No. eabm7364.

(29) Kodanek, T.; Freytag, A.; Schlosser, A.; Naskar, S.; Härtling, T.; Dorfs, D.; Bigall, N. C. Macroscopic Aerogels with Retained Nanoscopic Plasmonic Properties. *Z. Phys. Chem.* **2018**, *232*, 1675−1689.

(30) Wen, D.; Liu, W.; Haubold, D.; Zhu, C.; Oschatz, M.; Holzschuh, M.; Wolf, A.; Simon, F.; Kaskel, S.; Eychmuller, A. Gold Aerogels: Three-Dimensional Assembly of Nanoparticles and Their Use as Electrocatalytic Interfaces. *ACS Nano* **2016**, *10*, 2559−2567.

(31) Solis, D. M.; Taboada, J. M.; Obelleiro, F.; Liz-Marzan, L. M.; Garcia de Abajo, F. J. Toward Ultimate Nanoplasmonics Modeling. *ACS Nano* **2014**, *8*, 7559−7570.

(32) Fuller, K. A. Optical resonances and two-sphere systems. *Appl. Opt.* **1991**, *30*, 4716−4731.

(33) Mackowski, D. W.; Mishchenko, M. I. Calculation of the T matrix and the scattering matrix for ensembles of spheres. *J. Opt. Soc. Am. A* **1996**, *13*, 2266−2278.

(34) Mackowski, D. W.; Mishchenko, M. I. A multiple sphere T-matrix Fortran code for use on parallel computer clusters. *J. Quant. Spectrosc. Radiat. Transfer* **2011**, *112*, 2182−2192.

(35) Egel, A.; Pattelli, L.; Mazzamuto, G.; Wiersma, D. S.; Lemmer, U. CELES: CUDA-accelerated simulation of electromagnetic scattering by large ensembles of spheres. *J. Quant. Spectrosc. Radiat. Transfer* **2017**, *199*, 103−110.

(36) Pattelli, L.; Egel, A.; Lemmer, U.; Wiersma, D. S. Role of Packing Density and Spatial Correlations in Strongly Scattering 3D Systems. *Optica* **2018**, *5*, 1037−1045.

(37) Zhao, L.; Kelly, L.; Schatz, G. C. The Extinction Spectra of Silver Nanoparticle Arrays: Influence of Array Structure on Plasmon Resonance Wavelength and Width. *J. Phys. Chem. B* **2003**, *107*, 7343−7350.

(38) Manjavacas, A.; Zundel, L.; Sanders, S. Analysis of the Limits of the Near-Field Produced by Nanoparticle Arrays. *ACS Nano* **2019**, *13*, 10682−10693.

(39) Cuartero-Gonzalez, A.; Sanders, S.; Zundel, L.; Fernandez-Dominguez, A. I.; Manjavacas, A. Super- and Subradiant Lattice Resonances in Bipartite Nanoparticle Arrays. *ACS Nano* **2020**, *14*, 11876−11887.

(40) Colomer-Ferrer, O.; Cosi, S. T.; Conti, Y.; Medina-Quiroz, D. E.; Scarabelli, L.; Mihi, A. Pre- and Post-assembly Modifications of Colloidal Plasmonic Arrays: the Effect of Size Distriution, Composition, and Annealing. *J. Mater. Chem. C* **2022**, *10*, 13913−13921.

(41) Rotne, J.; Prager, S. Variational treatment of hydrodynamic interaction in polymers. *J. Chem. Phys.* **1969**, *50*, 4831−4837.

https://doi.org/10.1021/acs.nanolett.3c00429
Nano Lett. 2023, 23, 3030−3037

(42) Fiore, A. M.; Balboa Usabiaga, F.; Donev, A.; Swan, J. W. Rapid sampling of stochastic displacements in Brownian dynamics simulations. *J. Chem. Phys.* **2017**, *146*, 124116.
(43) Keaveny, E. E.; Maxey, M. R. Modeling the magnetic interactions between paramagnetic beads in magnetorheological fluids. *J. Comput. Phys.* **2008**, *227*, 9554−9571.
(44) Sherman, Z. M.; Ghosh, D.; Swan, J. W. Field-directed self-assembly of mutually polarizable nanoparticles. *Langmuir* **2018**, *34*, 7117−7134.
(45) Lindbo, D.; Tornberg, A.-K. Spectral Accuracy in Fast Ewald-based Methods for Particle Simulations. *J. Comput. Phys.* **2011**, *230*, 8744−8761.
(46) Song, J.; Lu, C.-C.; Chew, W. C. Multilevel Fast Multipole Algorithm for Electromagnetic Scattering by Large Complex Objects. *IEEE Trans. Antennas Propag.* **1997**, *45*, 1488−1493.
(47) Taboada, J. M.; Araújo, M. G.; Basteiro, F. O.; Rodríguez, J. L.; Landesa, L. MLFMA-FFT Parallel Algorithm for the Solution of Extremely Large Problems in Electromagnetics. *Proc. IEEE* **2013**, *101*, 350−363.
(48) Shevchenko, E. V.; Talapin, D. V.; Kotov, N. A.; O'Brien, S.; Murray, C. B. Structural Diversity in Binary Nanoparticle Superlattices. *Nature* **2006**, *439*, 55−59.
(49) Young, K. L.; Ross, M. B.; Blaber, M. G.; Rycenga, M.; Jones, M. R.; Zhang, C.; Senesi, A. J.; Lee, B.; Schatz, G. C.; Mirkin, C. A. Using DNA to design plasmonic metamaterials with tunable optical properties. *Adv. Mater.* **2014**, *26*, 653−659.
(50) Schimpf, A. M.; Lounis, S. D.; Runnerstrom, E. L.; Milliron, D. J.; Gamelin, D. R. Redox chemistries and plasmon energies of photodoped In_2O_3 and Sn-doped In_2O_3 (ITO) nanocrystals. *J. Am. Chem. Soc.* **2015**, *137*, 518−524.
(51) Gibbs, S. L.; Staller, C. M.; Agrawal, A.; Johns, R. W.; Saez Cabezas, C. A.; Milliron, D. J. Intrinsic Optical and Electronic Properties from Quantitative Analysis of Plasmonic Semiconductor Nanocrystal Ensemble Optical Extinction. *J. Phys. Chem. C* **2020**, *124*, 24351−24360.
(52) Del Gado, E.; Kob, W. Structure and relaxation dynamics of a colloidal gel. *Europhys. Lett.* **2005**, *72*, 1032−1038.
(53) Sherman, Z. M.; Howard, M. P.; Lindquist, B. A.; Jadrich, R. B.; Truskett, T. M. Inverse methods for design of soft materials. *J. Chem. Phys.* **2020**, *152*, 140902.
(54) Kang, J.; Sherman, Z. M.; Crory, H. S. N.; Conrad, D. L.; Berry, M. W.; Roman, B. J.; Anslyn, E. V.; Truskett, T. M.; Milliron, D. J. Modular Mixing in Plasmonic Metal Oxide Nanocrystal Gels with Thermoreversible Links. *J. Chem. Phys.* **2023**, *158*, 024903.
(55) Singh, M.; Sherman, Z. M.; Milliron, D. J.; Truskett, T. M. Linker-Templated Structure Tuning of Optical Response in Plasmonic Nanoparticle Gels. *J. Phys. Chem. C* **2022**, *126*, 16885−16893.
(56) Kim, Y.; Yeom, B.; Arteaga, O.; Yoo, S. J.; Lee, S.-G.; Kim, J.-G.; Kotov, N. A. Reconfigurable chiroptical nanocomposites with chirality transfer from the macro-to the nanoscale. *Nat. Mater.* **2016**, *15*, 461−468.

https://doi.org/10.1021/acs.nanolett.3c00429
Nano Lett. 2023, 23, 3030−3037